Physics of Fluids

Energy harvesting through flow-induced oscillations of a foil

Cite as: Phys. Fluids **21**, 123602 (2009); https://doi.org/10.1063/1.3275852
Submitted: 20 July 2009 . Accepted: 29 October 2009 . Published Online: 22 December 2009

Zhangli Peng, and Qiang Zhu


View Online


Export Citation

ARTICLES YOU MAY BE INTERESTED IN

Mode coupling and flow energy harvesting by a flapping foil
Physics of Fluids **21**, 033601 (2009); https://doi.org/10.1063/1.3092484

Inertial effects of the semi-passive flapping foil on its energy extraction efficiency
Physics of Fluids **27**, 053103 (2015); https://doi.org/10.1063/1.4921384

Ambient wind energy harvesting using cross-flow fluttering
Journal of Applied Physics **109**, 026104 (2011); https://doi.org/10.1063/1.3525045

AIP Publishing

© 2009 American Institute of Physics.

Energy harvesting through flow-induced oscillations of a foil

Zhangli Peng and Qiang Zhu[a)]
Department of Structural Engineering, University of California, San Diego, La Jolla, California 92093, USA

(Received 20 July 2009; accepted 29 October 2009; published online 22 December 2009)

By using a Navier–Stokes model, we examine a novel flow energy harvesting device consisting of a flapping foil mounted on a damper (representing the power generator) and a rotational spring. Self-induced and self-sustained flapping motions, including a heaving motion $h(t)$ and a pitching motion $\alpha(t)$, are excited by an incoming flow and power extraction is achieved from the heaving response. Depending upon the configuration of the system and the mechanical parameters (e.g., the location of the pitching axis and the stiffness of the rotational spring), four different responses are recorded: (i) the foil remains stable in its initial position ($\alpha=0$ and $h=0$); (ii) periodic pitching (around $\alpha=0$) and heaving motions are excited; (iii) the foil undergoes irregular motions characterized by switching between oscillations around two pitching angles; and (iv) the foil rotates to a position with an angle to the incoming flow and oscillates around it. The existence of response (ii) suggests the feasibility of controllable and stable flow energy extraction by this device. Through numerical simulations with a Navier–Stokes model we have determined combinations of geometric and mechanical parameters to achieve this response. The corresponding energy harvesting capacity and efficiency are predicted. © *2009 American Institute of Physics*. [doi:10.1063/1.3275852]

I. INTRODUCTION

Traditionally, energy extraction from wind and current has been achieved through turbine-based devices containing rotating blades. This particular design may lead to inborn structural weakness associated with centrifugal stress. High-performance (light and strong) materials are necessary and thus the costs are increased. Moreover, in conventional designs, e.g. the horizontal axis wind turbines, large translational speed is reached at the tips of the blades. In large wind turbines, this speed approaches the sound barrier causing serious environmental concerns about noise generation as well as the threat they pose to birds. Other flow energy extraction devices, e.g., dams and water wheels, are also harmful to the environment by blocking passages of migratory fishes.

In recent years, a new type of flow energy recovery paradigm characterizing unsteady motions of hydro- or aerofoils has been tested. The basic principle of this device relies upon fluid-induced vibrations. Its feasibility has been demonstrated through scaled models and prototypes.[1] Stemming from investigations of biolocomotion mechanisms of aquatic animals and insects, these bioinspired apparatuses promise mitigated impact upon the environment.

The fundamental mechanisms of flow energy harvesting through oscillating foils have been studied for several decades. It was originally demonstrated that a flapping foil was capable of extracting energy from an oscillating current.[2,3] Further studies showed that a stationary foil, while submerged under incoming waves, could propel itself forward using energy extracted from the wave-generated flow.[4,5] Energy harvesting by a flapping foil from a uniform flow has also been investigated.[6] Existing studies mostly focused upon flow-body interaction mechanisms (e.g., vortex generation and vortex-body interaction) that affect energy exchange between the incoming flow and a foil undergoing prescribed oscillations.[7–9] According to these investigations, if both heaving and pitching motions are accurately controlled, in optimal cases the energy extraction efficiency (defined as the portion of the flow energy flux through the area swept by the foil extracted by the device) reaches 50%,[9] approaching the Betz limit.[10]

In practice, it is necessary to identify measures to achieve the combined heaving and pitching motions for flow energy harvesting from a uniform flow. Towards this end, recent studies concentrated upon hydrodynamic mode coupling,[11–13] in which one of the oscillation modes (e.g., pitching) is actuated and another mode (e.g., heaving) is excited by variations of the hydrodynamic forces and moments. Using a linearized thin-plate model, it was demonstrated that via this mechanism positive power extraction (the extracted power subtracting the power required for activation) was obtained over a large range of geometric, mechanical, and operational parameters. It was also showed that when the pitching motion was harmonic, the upper limit of the power extraction was $(\pi/8)\rho a\alpha_0^2 U^3$ (measured per unit span length), where ρ is the density of the fluid, a is the chord length of the foil, U is the speed of the flow, and α_0 is the amplitude of pitching.[12] Further simulations with a Navier–Stokes model illustrated that the performance of the system was closely related to vorticity control mechanisms, in particular the interaction between the leading-edge vortices (LEV) and the foil.[13]

To avoid the complicated control and activation systems and further simplify the design, we herein propose a purely passive device relying on self-induced and self-sustained oscillations for energy generation. Rather than actively control-

[a)]Author to whom correspondence should be addressed. Electronic mail: qizhu@ucsd.edu. Telephone: +1-858-822-2161. Fax: +1-858-822-2260.

 © 2009 American Institute of Physics

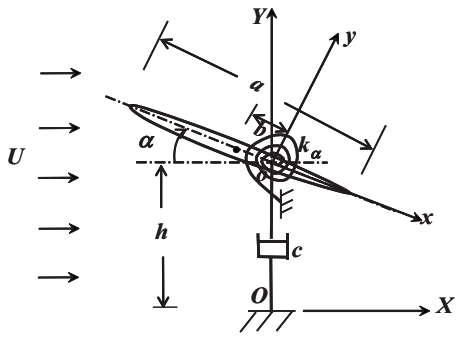

FIG. 1. Schematic of the flapping foil energy harvester.

ling the pitching motion, the foil motion will be completely excited by flow-induced instability (the same mechanism responsible for flutter of airfoils). The basic design involves a foil mounted on a simple structural system containing a rotational spring in the pitching direction and a damper in the heaving direction. When flow-induced oscillations occur, a combination of pitching and heaving motions is excited and power is extracted from the heaving motion through the damper. To achieve this, several critical issues need to be clarified, including (1) through self-induced vibrations, is it possible to achieve predictable and controllable foil motions essential for stable energy production? (2) If so, within what range of geometric and mechanical parameters is this flapping pattern obtained? (3) What will be the energy harvesting performance (characterized by the power extraction capacity and efficiency) of this device?

To answer these questions, in this study we apply a two-dimensional Navier–Stokes model to solve the fluid-structure interaction problem involved in the aforementioned design and investigate the dynamics and energy harvesting performance of the system at different combinations of parameters.

The rest of the paper is organized as follows. We first describe the physical problem and the mathematical formulation. A linear stability analysis based upon a thin-plate model is conducted for an estimate of the possible parameter range within which flow-induced oscillation can be excited. The system is then solved with the Navier–Stokes model and its dynamic responses, especially the energy recovery capacity, are accurately predicted. Finally, conclusions are drawn.

II. PROBLEM FORMULATIONS

A. Problem description

As shown in Fig. 1, we consider a foil with two degrees of freedom (heave and pitch) immersed in a uniform incoming flow U. The chord length of the foil is a. At an axis located at a distance b from the center, the foil is attached to a rotational spring k_α in the pitching direction and a viscous damper c in the heaving direction.

Assuming that the mass and the rotational inertia of the foil are negligible, the equations of motion are expressed as

$$c\dot{h} = L, \tag{1}$$

$$k_\alpha \alpha = -M, \tag{2}$$

where h depicts the heaving motion and α the angle of attack. L and M are the hydrodynamic lifting force and pitching moment, respectively.

In this apparatus, the damper c acts as a generator, from which a power output is achieved as $P=c\dot{h}^2$. In periodic foil motions we concentrate upon the average power extraction defined as $\bar{P}=(1/T)\int_{t_0}^{t_0+T} P dt$, where T is the fundamental period of motion. The power harvesting efficiency, another important index of performance, is defined as the portion of flow energy flux within the swept area extracted by the device, i.e., $\eta=\bar{P}/\frac{1}{2}\rho U^3 Y_p$ (where Y_p is calculated as the difference between the highest and the lowest vertical positions reached by the leading/trailing edges).

For normalization, hereafter we assume that $a=1$, $U=1$, and the fluid density $\rho=1$. To reduce the number of variables, we also assume that the normalized damping coefficient $c=\pi$, where high performance in terms of energy harvesting has been recorded in previous studies.[12,13]

B. Linear stability analysis

As a guidance for the Navier–Stokes simulations that follow, we first carry out a stability analysis based upon a reduced hydrodynamics model to estimate the range of parameters (i.e., b and k_α) within which self-induced vibration can be excited.

Following Theodorsen,[14] we depict the hydrodynamic lifting force L and the hydrodynamic pitching moment M in Eqs. (1) and (2) as combinations of the quasisteady lifting force and pitching moment, the added-mass force and moment, and the adjustments due to wake formation. Mathematically, L and M are written as

$$L = \pi[-\dot{h} + \alpha + (1/4 - b)\dot{\alpha}]C(\Omega) + \frac{\pi}{4}(-\ddot{h} + \dot{\alpha} - b\ddot{\alpha}), \tag{3}$$

$$M = \frac{\pi}{16}\dot{\alpha} - \frac{\pi}{4}[-\dot{h} + \alpha + (1/4 - b)\dot{\alpha}]C(\Omega) + \frac{\pi}{128}\ddot{\alpha} - Lb. \tag{4}$$

In the expressions above, $C(\Omega)$ is the deficiency factor representing effects of vorticity shedding from the trailing edge (which depends upon the frequency Ω). Mathematically, we have

$$C(\Omega) = \frac{K_1(i\Omega/2)}{K_0(i\Omega/2) + K_1(i\Omega/2)} = \frac{H_1^{(2)}(\Omega/2)}{H_1^{(2)}(\Omega/2) + H_0^{(2)}(\Omega/2)}, \tag{5}$$

where $i=\sqrt{-1}$. K_n $(n=0,1)$ is the modified Bessel function of the second kind. $H_n^{(2)}$ $(n=0,1)$ is the Hankel function of the second kind.

In order to analyze the stability of this system, we assume that there exists a solution in the form of $h(t)=h_0 e^{\gamma t}$ and $\alpha(t)=\alpha_0 e^{\gamma t}$. Substituting these into Eqs. (1) and (2), we obtain an eigenvalue equation

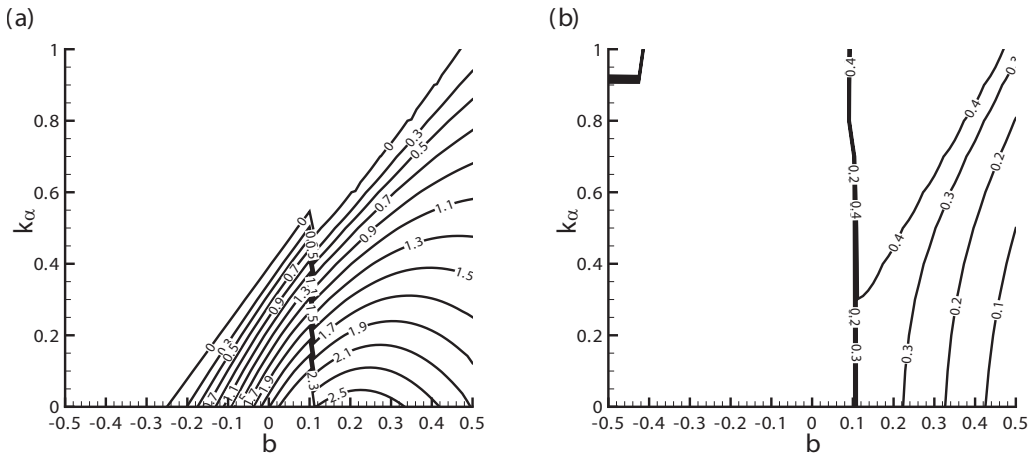

FIG. 2. (a) Real part and (b) imaginary part of the root γ_1.

$$\begin{bmatrix} a_{11}(\gamma) & a_{12}(\gamma) \\ a_{21}(\gamma) & a_{22}(\gamma) \end{bmatrix} \begin{bmatrix} h_0 \\ \alpha_0 \end{bmatrix} = \begin{bmatrix} 0 \\ 0 \end{bmatrix}, \tag{6}$$

where a_{11}, a_{12}, a_{21}, and a_{22} are expressed as

$$a_{11} = [c + \pi C(\Omega)]\gamma\frac{\pi}{4}\gamma^2,$$

$$a_{12} = -\pi C(\Omega) - \left[\pi\left(\frac{1}{4} - b\right)C(\Omega) + \frac{\pi}{4}\right]\gamma + \frac{\pi}{4}b\gamma^2,$$

$$a_{21} = \left(\frac{1}{4} + b\right)\pi C(\Omega)\gamma\frac{\pi}{4}b\gamma^2,$$

$$a_{22} = k_\alpha - \left(\frac{1}{4} + b\right)C(\Omega) - \left[-\frac{\pi}{16} + \left(\frac{1}{16} - b^2\right)\pi C(\Omega) + \frac{b\pi}{4}\right]\gamma + \left(\frac{1}{128} + \frac{b^2}{4}\right)\pi\gamma^2.$$

In order for there to be nonzero solutions of h_0 and α_0, the condition $a_{11}a_{22} - a_{12}a_{21} = 0$ has to be satisfied. It yields three nonzero solutions of γ: γ_1, γ_2, and γ_3. Our calculations show that among these the only one that may have a positive real part (an indication of instability) is γ_1. To ensure that the frequency we apply to calculate the deficiency factor C is consistent with the frequency of this unstable mode, we replace Ω with $|\mathrm{Im}(\gamma_1)|$ and recalculate γ_1 following the above-discussed procedure. Convergence is achieved after a few iterations.

The solutions of the real and imaginary parts of γ_1 are shown in Fig. 2. Instability occurs when b is larger than -0.25 (negative values of b correspond to cases when the pitching axis is located in front of the center of the foil), i.e., the pitching axis is behind the 1/4 chord point. For each b there exists a critical k_α beyond which the system is stabilized by the rotational spring. The value of this critical k_α increases with b. In the vicinity of $b \sim 0.1$ the imaginary part of γ_1 jumps from small (but nonzero) values to $O(1)$ values [Fig. 2(b)]. Correspondingly abrupt changes in the real part of γ_1 are also observed [Fig. 2(a)].

This linear stability analysis suggests that when b is larger than -0.25 and k_α is sufficiently small the system might become unstable, making it possible for flow energy harvesting. The remaining questions are the following: (1) what will be the response of the system when instability occurs? (2) under what conditions can we achieve controllable foil motions essential for stable energy extraction? and (3) what will be the performances (energy harvesting capacity and efficiency) of the system? To answer these questions, we herein implement a fully viscous, fully nonlinear fluid-structure interaction model.

III. NUMERICAL METHOD

To numerically solve the finite Reynolds number flow around the foil and determine the hydrodynamic lifting force L and pitching moment M in Eqs. (1) and (2), we apply a two-dimensional Navier–Stokes model originally reported by Guglielmini and Blondeaux.[15] The same method has been employed in our previous work to investigate flow energy recovery by flapping foils through hydrodynamic mode coupling.[13] The key procedure of this model is summarized below while details are not included for brevity.

A. Mathematical formulation and numerical model of the flow around the foil

As plotted in Fig. 1, the problem formulation is performed within a dual-coordinate system including a space-fixed Euler reference frame $(O-XY)$ and a body-fixed Lagrangian frame $(o-xy)$. These two reference frames are related through a translational/rotational transformation, i.e.,

$$\begin{bmatrix} x \\ y \end{bmatrix} = \begin{bmatrix} \cos\alpha & -\sin\alpha \\ \sin\alpha & \cos\alpha \end{bmatrix} \begin{bmatrix} X \\ Y - h \end{bmatrix}. \tag{7}$$

For convenience we assume that the foil has a

Joukowski profile, which is easily mapped into a circle with radius $\lambda+e+s$ in a (μ,ν) plane through the Joukowski transformation expressed as

$$\mathbf{x}=\mathbf{z}+\frac{\lambda^2}{\mathbf{z}-e}+d-e, \tag{8}$$

where $\mathbf{x}=x+iy$ and $\mathbf{z}=\mu+i\nu$. e and s are parameters characterizing the thickness of the foil and the sharpness of the trailing edge, respectively. d determines the location of the pitching axis o, which is given as $d=(\lambda+2e+s)+\lambda^2/(\lambda+2e+s)-(1/2+b)$. Following the normalization, λ, e, and s are chosen so that the chord length of the foil, $2(\lambda+e+s)+\lambda^2/(\lambda+s)+\lambda^2/(\lambda+2e+s)$, equals 1; in our simulations we choose $\lambda=0.2486$ and $e=s=0.0124$.

The Navier–Stokes equations, expressed in the vorticity-stream function $(\omega-\psi)$ format, are given as

$$\frac{\partial(J\omega)}{\partial t}+\sqrt{J}\mathbf{u}\cdot\nabla\omega=\frac{1}{R_{e\lambda}}\nabla^2\omega, \tag{9}$$

and

$$\nabla^2\psi=-J\omega, \tag{10}$$

where $J=1+\{1-2[(\mu-e)^2-\nu^2]\}/[(\mu-e)^2+\nu^2]^2$ represents the Jacobian of the transformation $(\mu,\nu)\rightarrow(x,y)$. $\mathbf{u}$ is the flow velocity. $R_{e\lambda}\equiv R_e\lambda$, where R_e is the Reynolds number based upon the chord length and the incoming flow speed.

Furthermore, we define a cylindrical coordinate system (r,θ) within the (μ,ν) plane so that $r=\sqrt{\mu^2+\nu^2}$ and $\theta=\tan^{-1}(\nu/\mu)$. We rewrite the Navier–Stokes Eqs. (9) and (10) in (r,θ) by using $\nabla=[(\partial/\partial r),(1/r)(\partial/\partial\theta)]$, $\nabla^2=(\partial^2/\partial r^2)+(1/r)(\partial/\partial r)+(1/r^2)(\partial^2/\partial\theta^2)$, and $\mathbf{u}=(u_r,u_\theta)$, where

$$u_r=\frac{1}{\sqrt{J}}\left[\frac{1}{r}\frac{\partial\psi}{\partial\theta}-(-\dot{h}\sin\alpha+\dot{\alpha}y)\left(\frac{\partial x}{\partial\mu}\cos\theta+\frac{\partial x}{\partial\nu}\sin\theta\right)-(\dot{h}\cos\alpha-\dot{\alpha}x)\left(\frac{\partial y}{\partial\mu}\cos\theta+\frac{\partial y}{\partial\nu}\sin\theta\right)\right], \tag{11}$$

$$u_\theta=\frac{1}{\sqrt{J}}\left[-\frac{\partial\psi}{\partial r}-(-\dot{h}\sin\alpha+\dot{\alpha}y)\left(-\frac{\partial x}{\partial\mu}\sin\theta+\frac{\partial x}{\partial\nu}\cos\theta\right)-(\dot{h}\cos\alpha-\dot{\alpha}x)\left(-\frac{\partial y}{\partial\mu}\sin\theta+\frac{\partial y}{\partial\nu}\cos\theta\right)\right]. \tag{12}$$

The boundary-value problem is completed by applying the boundary conditions; on the surface of the foil, we apply the no-flux and the no-slip boundary conditions so that the velocity components measured in the moving coordinate system disappear; in the far field $(r\rightarrow\infty)$ the flow field is assumed to be undisturbed at the inflow boundaries, while a vanishing normal derivative of the vorticity is enforced at the outflow boundaries.[15]

The Navier–Stokes equations together with the boundary conditions are solved with a finite difference algorithm through discretizations in r, θ, and t. For better resolution of the boundary layer near the foil surface, we further define a variable $z\equiv\ln(r+r_0)$ and apply N_r evenly distributed grids along z. The parameter r_0 can be adjusted so that the sizes of the grids close to the foil surface are much smaller than the boundary-layer thickness to maintain sufficient resolution.[15,16] During time integration, the vorticity field ω is updated at each time step by numerically integrating the vorticity Eq. (9) via an alternative direction implicit algorithm. Afterwards the Poisson Eq. (10) is solved by using an efficient spectral method.

Details of the mathematical formulation, as well as model validations through comparisons with experimental and numerical results, are found in Zhu and Peng[13] (and also in Guglielmini and Blondeaux[15]).

B. Hydrodynamic forces and moments

With the near-body flow field resolved, the hydrodynamic force $\mathbf{F}$ is given as [see, e.g., Eldredge 2007 (Ref. 17)]

$$\mathbf{F}=\frac{1}{R_e}\oint_{S_b}\left[(\mathbf{X}-\mathbf{X}_o)\times\frac{\partial\boldsymbol{\omega}}{\partial n}-\mathbf{n}\times\boldsymbol{\omega}\right]ds+A\ddot{h}\mathbf{e}_Y, \tag{13}$$

where $\mathbf{X}\equiv(X,Y)$ represents a point on the foil surface. $\boldsymbol{\omega}\equiv\omega\mathbf{e}_Z$. $\mathbf{e}_Z$ is the unit vector in the Z (pointing out of the plane) direction. $\mathbf{e}_Y$ is the unit vector in the Y direction. $\mathbf{n}$ is the unit surface normal vector pointing into the body. $\mathbf{X}_o$ is the location of the pitching axis. A is the area of the body. The integration is performed around the body surface S_b. The lifting force L corresponds to the Y component of $\mathbf{F}$.

Similarly, the hydrodynamic moment with respect to the pitching axis is obtained as

$$M=\frac{1}{R_e}\oint_{S_b}(\mathbf{X}-\mathbf{X}_o)\times\left[\frac{1}{2}(\mathbf{X}-\mathbf{X}_o)\times\frac{\partial\boldsymbol{\omega}}{\partial n}-\mathbf{n}\times\boldsymbol{\omega}\right]\cdot\mathbf{e}_Z ds+\frac{4}{R_e}A\dot{\alpha}-\ddot{\alpha}(A|\mathbf{X}-\mathbf{X}_o|^2+2B)+A\ddot{h}\mathbf{e}_Z\cdot[(\mathbf{X}-\mathbf{X}_o)\times\mathbf{e}_Y], \tag{14}$$

where B is the second area moment of inertia of the body.

C. Fluid-structure interactions

For simultaneous simulation of the flow field and the mechanical response of the system as depicted by Eqs. (1) and (2), we rely upon an iteration algorithm.[13] To elaborate, at each time step, the following iteration procedure is conducted: (1) starting from an initial guess of the heaving position h_1 and velocity $\dot{h}_1$, as well as the pitching position α_1 and velocity $\dot{\alpha}_1$ (usually these are prescribed as the values in the previous time step), the hydrodynamic problem is solved, from which the hydrodynamic lifting force L and the pitching moment M are calculated; (2) by numerically integrating Eqs. (1) and (2), we obtain the updated values of the heaving position h_2 and velocity $\dot{h}_2$, and the pitching position α_2 and velocity $\dot{\alpha}_2$; and (3) if these values are not sufficiently close to the initial guess, we use them as the new guess and repeat steps 1–2.

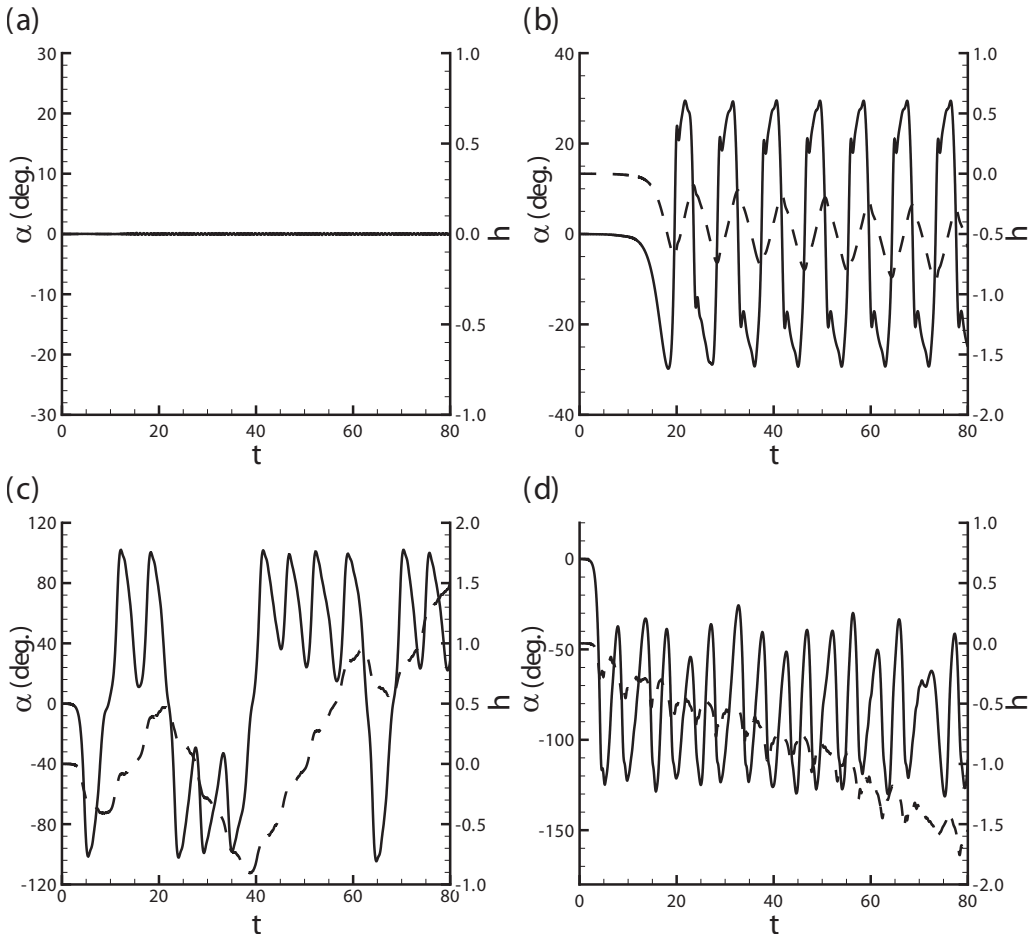

FIG. 3. Variations of the angle of attack α (solid lines) and heave h (dashed lines) at four different cases: (a) $b=-0.2$, $k_\alpha=0.1$; (b) $b=-0.2$, $k_\alpha=0$; (c) $b=0$, $k_\alpha=0.012$; and (d) $b=0$, $k_\alpha=0$.

It is well-known that instability arises when the added-mass effect dominates the system's response. In order to eliminate this instability and to accelerate the convergence of the aforementioned iteration algorithm, we apply an implicit added-mass method by subtracting the hydrodynamic force due to added mass ($-m_a\ddot{h}$, where m_a is the added mass) and the hydrodynamic moment due to added pitching inertia from both sides of the motion equations. For example, during iteration step i we replace Eq. (1) with $m_a\ddot{h}_{i+1}+c\dot{h}_{i+1}=L+m_a\ddot{h}_i$. Equation (2) is reformatted in a similar manner by using an added inertia I_a. Although it is difficult to accurately predict m_a and I_a, these values do not affect the accuracy of the results as long as convergence is achieved.

IV. RESULTS

By using the Navier–Stokes model, we systematically study dynamics of the flapping-foil system in response to uniform incoming flows. In the following simulations, we choose $R_e=1000$. To expedite the growth of instability, at the initial stage ($t<0.8$) a disturbance in the form of a sinusoidal pitching moment with amplitude 10^{-3} and period 0.8 is applied.

A. Dynamic behaviors of the system

Our study shows that depending upon b and k_α, the system displays four distinctive dynamic behaviors. First, when b is close to -0.5 (i.e., the pitching axis is close to the leading edge) and/or k_α is sufficiently large, the foil remains stationary at $\alpha=0$ [Fig. 3(a)]. Second, the foil undergoes periodic pitching and heaving motions around $\alpha=0$ [Fig. 3(b)]. This scenario is ideal for energy extraction. Third, the pitching motion of the foil switches between two oscillating states, one corresponding to oscillation around α_0 ($\alpha_0\neq 0$) and the other around $-\alpha_0$ [Fig. 3(c)] (note that the value of α_0 is case dependent). In this scenario the motion is highly irregular. Finally, the system stays at one of these oscillatory states and the irregularity of motion is greatly reduced [Fig. 3(d)].

In Fig. 3(b), the spikes in the time history of the pitching motion are attributed to interactions between the LEV and the foil itself. As shown in Fig. 4 (in this figure and in the following figures, the white areas correspond to counter-clockwise vortices and the dark areas the clockwise vortices), vortices generated at the leading-edge area travel downstream and may collide with the trailing part of the foil (e.g., at $t=T/8$). This is reminiscent of performance enhancement

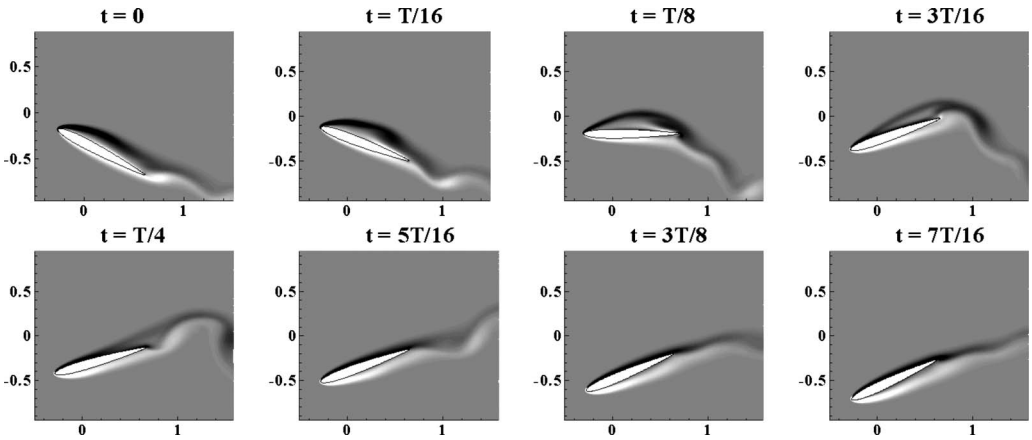

FIG. 4. Evolution of the near-body flow (vorticity contour) within half of the fundamental period T at $b=-0.2$ and $k_\alpha=0$.

associated with recovery of the LEV energy in flow energy harvesting based on hydrodynamic mode coupling. It has been demonstrated that depending upon the relative motions of the LEV and the foil, the LEV energy could either be strengthened or partly recovered at the trailing edge.[13] The former scenario leads to a stronger wake, while the latter scenario increases the energy harvesting capacity of the system. In the particular case shown in Fig. 4 at $t\sim T/8$, the induced moment of the LEV coincides with the direction of the instantaneous pitching motion so that the LEV-foil interaction enhances energy recovery.

Keeping $k_\alpha=0$, when b increases from -0.2 to -0.1 the pitching amplitude increases from 30° to 87°, accompanied by significant increase in LEV (Fig. 5). Indeed, in this case LEV dominates the flow field. During the half period shown in the figure, a strong LEV is generated at $\alpha\sim-87°$ and a relatively weak LEV is created at $\alpha\sim0$, while vortices generated at the trailing edge are much weaker.

Through systematic simulations, we have located the boundaries between the four different dynamic behaviors within the $b-k_\alpha$ plane. As shown in Fig. 6, for a fixed b $(-0.2<b<0.5)$, when the rotational spring k_α is sufficiently strong the system remains stationary [hereafter tagged as response (i)]. A critical value of k_α exists, below which periodic oscillation around $\alpha=0$ [response (ii)], irregular motions characterized by mode switching between oscillations around $\pm\alpha_0$ [response (iii)], and oscillations around a certain nonzero angle [response (iv)] occur in succession with decreasing k_α.

According to this fully viscous simulation, the range of b within which flow-induced vibration can exist is consistent with the predictions by the reduced model. The critical value of k_α, on the other hand, is much smaller than the previous predictions so that the instability region within the $b-k_\alpha$ plane [i.e., responses (ii)–(iv)] is significantly diminished. Moreover, the discontinuity around $b=0.1$ does not appear in the Navier–Stokes results. This is possibly attributed to the stabilization effect of fluid viscosity, which is fully accounted for in the Navier–Stokes model but not in the reduced model. Other factors that contribute to the discrepancy are geometries of the foil (thin flat plate versus Joukowski foil), treatments of moving boundaries (linear versus fully nonlinear), and the inclusion of LEV.

The occurrence of these four responses is ultimately controlled by the existence of multiple equilibrium states in the system. For perspective we herein consider a special case within the potential-flow regime with $k_\alpha=0$. Considering

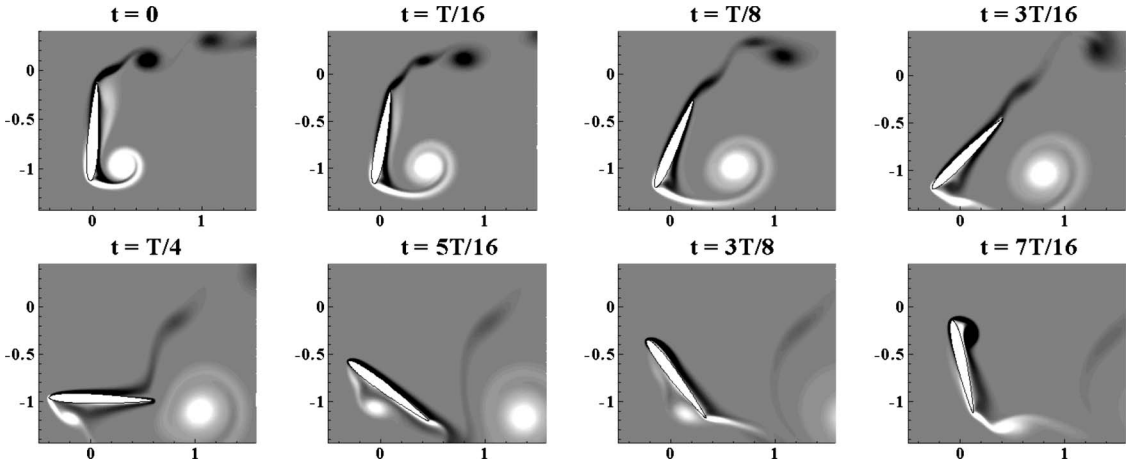

FIG. 5. Evolution of the near-body flow (vorticity contour) within half of the fundamental period T at $b=-0.1$ and $k_\alpha=0$.

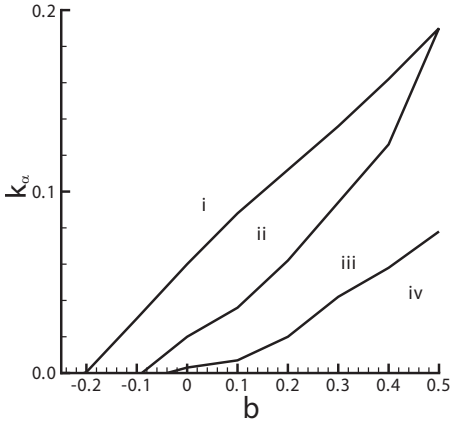

FIG. 6. Boundaries between the four system behaviors: (i) steady state at $\alpha=0$, (ii) periodic oscillations around $\alpha=0$, (iii) mode switching between oscillations around α_0 and $-\alpha_0$, and (iv) oscillations around α_0 ($\alpha_0 \neq 0$).

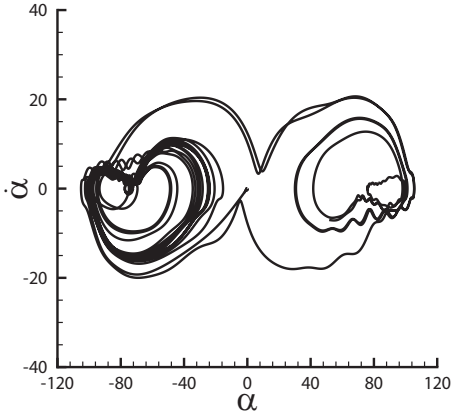

FIG. 8. Projection of the phase plane trajectory in the $\alpha-\dot{\alpha}$ plane showing competition between two oscillation modes. $b=-0.05$ and $k_\alpha=0$. The angles are shown in degrees.

Munk moment, at least four possible equilibrium states are identified: (a) the initial position $\alpha=0$, (b) $\alpha=90°$, (c) $\alpha=-90°$, and (d) $\alpha=180°$. The occurrence and stability of these equilibrium states depend on the location of the pitching axis. As the pitching axis is near the leading edge, the only stable equilibrium state is (a). Similarly, if the pitching axis is near the trailing edge the foil will stay at (d). When the pitching axis is located close to the center, however, both (b) and (c) become stable states while (a) and (d) are unstable.

When viscosity is included, unsteady hydrodynamics forces and moments associated with vortex shedding cause vibrations around one, or sometimes more than one, of the aforementioned equilibrium states. This is clearly demonstrated in our simulations. Indeed, responses (ii) and (iv) are both limit cycle responses. In Figs. 4 and 5, we see that when the pitching axis is close to the leading edge the system oscillates around equilibrium state (a). As b is further increased to 0, the equilibrium state (c) clearly dominates the response (Fig. 7). In this scenario the LEV is comparable in strength to vortices shed from the trailing edge. When b is between -0.1 and -0.04, the competition among multiple equilibrium states [e.g., (b) and (c)] leads to strange attractor behavior, causing mode switching and irregular responses (Fig. 8).

B. Energy harvesting capacity and efficiency

For energy harvesting purpose, hereafter we concentrate upon response (ii) (periodic oscillations around $\alpha=0$). We note that periodic motions are also achieved in response (iv). In fact, in cases within response (iv) [e.g. at $b=0.2$ and $k_\alpha=0$], the foil flips over by 180° and oscillates periodically around it. However, any nonzero k_α will disturb this type of response and cause transverse drifting. Thus these cases are not considered here.

A primary issue in energy harvesting is the robustness of the system, hereby referring to the sensitiveness of the responses to disturbances. To examine this, we have conducted simulations with different initial conditions, e.g., $\alpha=90°$ at

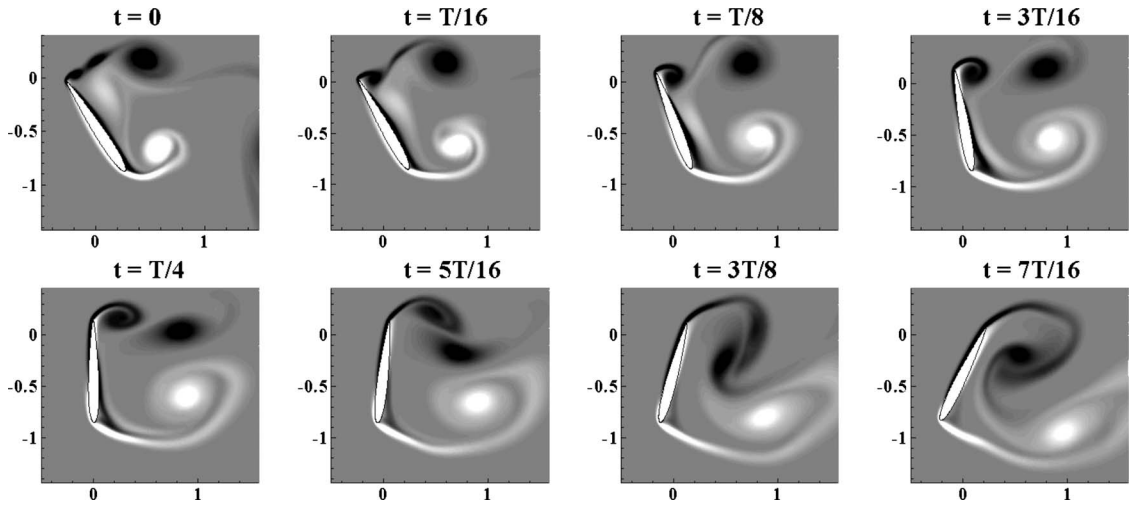

FIG. 7. Evolution of the near-body flow (vorticity contour) within half of the fundamental period T at $b=0$ and $k_\alpha=0$.

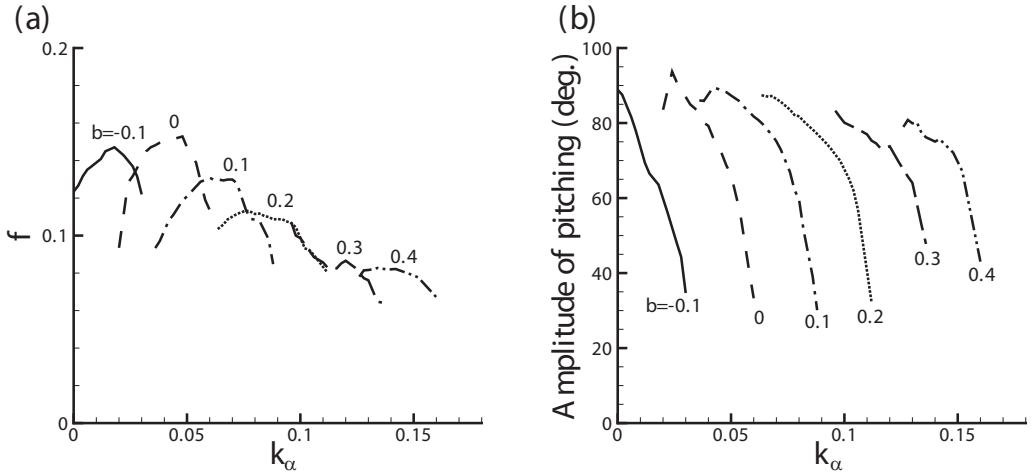

FIG. 9. (a) Frequency and (b) amplitude of the dominant pitching mode as functions of k_α at six different values of b.

$t=0$, and demonstrated that within response (ii) the response pattern is insensitive to disturbances. Indeed, in all the cases we study this periodic pattern is established within one fundamental period.

To illustrate the performance of the system within this region, we study its dynamics at six different locations of the axis, $b=-0.1$, 0, 0.1, 0.2, 0.3, and 0.4. Figure 9 demonstratesthe dependence of the dominant frequency (the inverse of the dominant period) and the amplitude of pitching at this frequency upon k_α within response (ii). It is seen that the frequency varies between 0.08 and 0.15, and the maximum amplitude of pitching is around 90°.

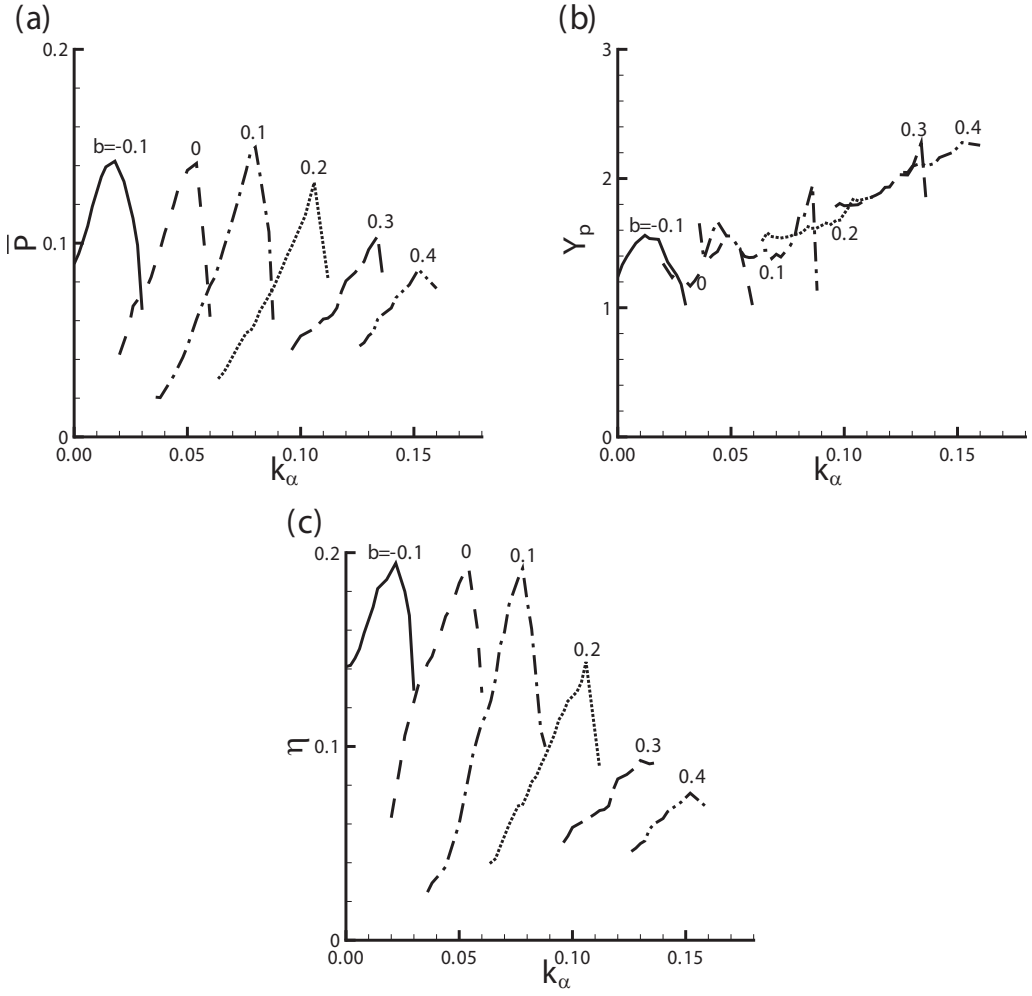

FIG. 10. (a) Mean power output, (b) swept distance, and (c) power extraction efficiency as functions of k_α at six different values of b.

In Fig. 10 we plot the mean power output $\bar{P}$, the swept distance Y_p, as well as the power extraction efficiency η as functions of k_α at these six different values of b. Interestingly, the peak performance of the system remains almost unchanged from $b=-0.1$ to $b=0.1$ ($\bar{P}\approx 0.14\sim 0.15$ and $\eta\approx 0.18\sim 0.20$), although they are achieved at different values of k_α (0.022, 0.054, and 0.078, respectively).

V. CONCLUSIONS

Although the flapping-foil flow energy harvester has clear advantages over traditional turbines with rotating blades in terms of environmental friendliness, its design and operation pose enormous challenges owing to the subtlety of the fluid-structure interaction problems involved. Indeed, as indicated by our current and previous studies (see for example, Refs. 12 and 13), unless properly designed and operated, such a system is unable to achieve power extraction from an incoming flow. This fact underscores the importance of accurately predicting its dynamic responses as well as the factors that may affect its performance. Towards this end we envisage a multistep approach including the following three procedures: (1) theoretical analysis and numerical modeling, (2) experiments with small scale models based upon conceptual designs tested in the first step, and (3) full scale model tests using prototypes that are optimally designed based upon the knowledge gained from the first two steps.

By using a Navier–Stokes model, in the current study we have investigated dynamics of a foil mounted on a rotational spring and a heaving damper in a uniform incoming flow. Unlike previous investigations in which the pitching motion is activated,[11–13] in this work the motion of the foil is passively generated by flow-induced instability so that the mechanical design is greatly simplified. Depending on the location of the pitching axis b and the stiffness of the rotational spring k_α, the system demonstrates four distinguishable behaviors, static response (no motion), periodic motion around $\alpha=0$, irregular motion characterized by mode switching between oscillations around two pitching angles, and oscillation around one (nonzero) pitching angle. Through systematic numerical simulations we have determined the boundaries between these responses within the $b-k_\alpha$ plane.

The primary purpose of this study is to investigate the feasibility of flow energy harvesting by fully passive flow-induced oscillations of a flapping foil. To achieve this we study dynamics of the system within the region of parameters where the foil undergoes periodic heaving and pitching motions around $\alpha=0$. Our simulations show that these self-induced regular motions are possible when b lies between -0.2 and 0.5 and k_α lies between an upper bound and a lower bound depending on b. It is also discovered that the energy harvesting capacity of the system remains stable as b varies from -0.1 to 0.1 (i.e., when the pitching axis is located close to the center of the foil). In optimal conditions, an energy harvesting efficiency of 20% is achieved.

A critical step is to characterize dynamics of the system at high Reynolds numbers (i.e., close to the range of Reynolds numbers in applications). As demonstrated in our analysis, the existence of different dynamic responses of the system is attributed to multiple equilibrium states in the dynamic system within the potential-flow regime. These states are not related to the viscosity of the fluid so that it is expected that the behavior of the system will not be qualitatively affected by the Reynolds number. Nevertheless, at high Reynolds numbers it is very likely that the performance of the system will be quantitatively different from our current predictions. To clarify this effect a combined investigation including numerical modeling of fluid-structure interactions with accurate turbulence modeling and laboratory experiments is necessary. Studies of the effects of three dimensionality as well as outer boundaries (e.g., ground effect) are also important.

[1] A. Westwood, "Ocean power: Wave and tidal energy review," Refocus **5**, 50 (2004).
[2] T. Y. Wu, "Extraction of flow energy by a wing oscillating in waves," J. Ship Res. **16**, 66 (1972).
[3] T. Y. Wu and A. T. Chwang, "Extraction of flow energy by fish and birds in a wavy stream," Proceedings of the Symposium on Swimming and Flying in Nature (Plenum Press, New York, 1975), Vol. 687.
[4] H. Isshiki and M. Murakami, "A theory of wave devouring propulsion," J. Soc. Nav. Archit. Jpn. **156**, 102 (1984).
[5] J. Grue, A. Mo, and E. Palm, "Propulsion of a foil moving in water waves," J. Fluid Mech. **186**, 393 (1988).
[6] W. McKinney and J. DeLaurier, "The wingmill: An oscillating-wing windmill," J. Energy **5**, 109 (1981).
[7] K. D. Jones and M. F. Platzer, "Numerical computation of flapping-wing propulsion and power extraction," AIAA Paper No. 97-0826, 1997.
[8] G. Dumas and T. Kinsey, "Eulerian simulations of oscillating airfoils in power extraction regime," *Advances in Fluid Mechanics VI* (WIT, Southampton, 2006), p. 245.
[9] B. J. Simpson, S. Licht, F. S. Hover, and M. S. Triantafyllou, "Energy extraction through flapping foils," Proceedings of the 27th International Conference on Offshore Mechanics and Arctic Engineering (ASME, 2008), Paper No. OMAE-2008-58043.
[10] A. Betz, *Introduction to the Theory of Flow Machines* (Pergamon, Oxford, 1966).
[11] E. Shimizu, K. Isogai, and S. Obayashi, "Multiobjective design study of a flapping wing power generator," ASME J. Fluids Eng. **130**, 021104 (2008).
[12] Q. Zhu, M. Haase, and C. H. Wu, "Modeling the capacity of a novel flow-energy harvester," Appl. Math. Model. **33**, 2207 (2009).
[13] Q. Zhu and Z. Peng, "Mode coupling and flow energy harvesting by a flapping foil," Phys. Fluids **21**, 033601 (2009).
[14] T. Theodorsen, "General theory of aerodynamic instability and the mechanisms of flutter," National Advisory Committee for Aeronautics, Report No. 496, 1935.
[15] L. Guglielmini and P. Blondeaux, "Propulsive efficiency of oscillating foils," Euro. J. Mech. B/Fluids **23**, 255 (2004).
[16] Z. J. Wang, "Vortex shedding and frequency selection in flapping flight," J. Fluid Mech. **410**, 323 (2000).
[17] J. D. Eldredge, "Numerical simulation of the fluid dynamics of 2D rigid body motion with the vortex particle method," J. Comput. Phys. **221**, 626 (2007).